Semi-automated stand delineation in Mediterranean *Pinus sylvestris* plantations through segmentation of LiDAR data: the influence of pulse density.

Mª Ángeles Varo-Martínez[1], Rafael M. Navarro-Cerrillo [1*], Rocío Hernández-Clemente [1,2], Joaquín Duque-Lazo[1]

[1]Department of Forestry Engineering-DedroLab-TreeSatLab - University of Cordoba. Edf. Leonardo da Vinci, Campus de Rabanales, 14075 Cordoba, Spain

[2]Swansea University, Department of Geography, Singleton Park, Swansea SA2 8PP, UK

Lidar stand delineation in pine forests

*To whom correspondence may be addressed.

Rafael M. Navarro-Cerrillo

University of Cordoba

Crta. IV, km. 396, 14071

Córdoba, Spain

E-mail: rmnavarro@uco.es Phone: 0034 957218657

Abstract

Traditionally, forest-stand delineation has been assessed based on orthophotography. The application of LiDAR has improved forest management by providing high-spatial-resolution data on the vertical structure of the forest. The aim of this study was to develop and test a semi-automated algorithm for stands delineation in a plantation of *Pinus sylvestris* L. using LiDAR data. Three specific objectives were evaluated, i) to assess two complementary LiDAR metrics, Assmann dominant height and basal area, for the characterization of the structure of *P. sylvestris* Mediterranean forests based on object-oriented segmentation, ii) to evaluate the influence of the LiDAR pulse density on forest-stand delineation accuracy, and iii) to investigate the algorithms´ effectiveness in the delineation of *P. sylvestris* stands for map prediction of Assmann dominant height and basal area. Our results show that it is possible to generate accurate *P. sylvestris* forest-stand segmentations using multiresolution or mean shift segmentation methods, even with low-pulse-density LiDAR - which is an important economic advantage for forest management. However, eCognition multiresolution methods provided better results than the OTB (Orfeo Tool Box) for stand delineation based on dominant height and basal area estimations. Furthermore, the influence of pulse density on the results was not statistically significant in the basal area calculations. However, there was a significant effect of pulse density on Assmann dominant height [$F_{2,\ 9595} = 5.69$, $p = 0.003$].for low pulse density. We propose that the approach shown here should be considered for stand delineation in other large *Pinus* plantations in Mediterranean regions with similar characteristics.

Key words

LiDAR, pulse density, mean shift segmentation, multiresolution segmentation, forest-stand delineation, automatic stand delineation.

Introduction

In forest management, a stand defines an area occupied by a group of trees that is homogeneous - in terms of species composition, size, age, arrangement, and condition - and distinguishable from other growth forms on adjoining areas (O'Hara and Nagel, 2013). Precise stand delineation is needed to manage different uses of the forested area and its expected ecological and economic benefits and revenue. Moreover, strategic decisions, such as when, where, or how to apply a particular silvicultural treatment, are taken at stand level (Dechesne et al., 2016).

Forest-stand delineation traditionally has been assessed based on orthophotography (Burnett and Blaschke, 2003). However, the combination of field forest inventory and remote sensing data in cartographic and silvicultural stand delineation is becoming more common (McRoberts et al., 2014). Satellite imagery (e.g. SPOT, IKONOS, or QuickBird) or Color-Infrared (CIR) images (Leckie et al., 2003; Pekkarinen, 2004) and Light Detection And Ranging (LiDAR) data (Bouvier et al., 2015) are currently used in this process.

Additionally, the uncertainty introduced by traditional methods of stand delineation has been tackled by automatic algorithms based on image segmentation methods (Radoux and Defourny, 2007). These techniques run an algorithm which generates partitions of the image with similar properties (Blaschke et al., 2014). Most of the segmentation techniques are based on statistical methods (Webb, 2003), where object classes are represented by probability density functions. Those functions are defined over a predetermined attribute space using methods based on machine learning (Chi and Ersoy, 2005; Zhong et al., 2008), directed towards the learning of complex relationships among sample patterns, and structural methods (Centeno et al., 2003; Sagerer and Niemann, 2013) based on spatial patterns (Costa et al., 2010).

The application of LiDAR provides high-spatial-resolution data on the vertical structure of the forest (Wu et al., 2013) and it has been used to make precise measurements of forest inventory attributes (e.g., to estimate biomass, timber volume, basal area, stem number, mean diameter, or dominant height) (Næsset, 2002) in order to improve forest management (Ruiz et al., 2014). With the introduction of LiDAR into forest inventory assessment, an increasing number of studies have involved stand segmentation detection (Bouvier et al., 2015). Through time, these studies have shown increased analytical complexity, increased accuracy of results, and a focus on the use of LiDAR data alone. However, the specification of the fieldwork, sensor, and flight parameters for laser data acquisition must be optimized to develop accurate forest inventories and mapping (Magnussen et al., 2012). The LiDAR data acquisition specifications, such as scan angle, pulse density, footprint size, and scan pattern, influence directly the ability to derive information on the forest structure. However, such attributes must be decided before the forest survey (Ruiz et al., 2014). Among these parameters, the LiDAR data pulse density is one of the most significant with regard to accurate estimation of forest-stand attributes (Magnusson et al., 2007).

In Mediterranean pine forests, canopy cover metrics are the forest management priority variables (e.g., stem number, diameter, basal area, or dominant height). However, in addition to yield metrics (Lopatin et al., 2015; Martín-Alcón et al., 2015), other metrics such as horizontal canopy heterogeneity, open canopy forest, and stand patterns must be taken into account to assess silvicultural alternatives. To overcome these drawbacks, the selection of LiDAR acquisition parameters (e.g., pulse number) and meaningful metrics to describe stand structure, as well as delimitation stand segmentation techniques, could help to develop models for specific *Pinus* Mediterranean forests. Therefore, the objective of this study was to develop and test a semi-automated algorithm for stands delineation in a plantation of *Pinus sylvestris* L. using LiDAR data. Three specific objectives were identified, i) to assess two complementary LiDAR metrics, Assmann dominant height and basal area, for characterizion of the structure of *P. sylvestris* Mediterranean forests based on object-oriented segmentation (e.g. eCognition software and Orpheo ToolBox software), ii) to evaluate the influence of the LiDAR pulse density on forest stand delineation accuracy, and iii) to investigate the algorithms´ effectiveness with regard to delineation of *P. sylvestris* stands, by evaluating its performance in map prediction of Assmann dominant height and basal area.

Materials and Methods

Study area

The study area is located in "Sierra de Los Filabres" (37°13'20'' N, 2°35'40'' W, between 1600 and 2186 m.a.s.l.), hereafter abbreviated as Filabres, south-eastern Spain (Fig. S1, Supporting Material). The forest under study is a 40-year-old *Pinus sylvestris* (hereafter Scots pine) plantation covering 409 ha, established using subsoiling as ground preparation between 1970 and 1976. The planting density was 2000 trees ha^{-1} and the current density ranges between 342 and 1473 trees ha^{-1}. The basal area ranges from 11.05 to 47.31 m^{2} ha^{-1} (Table S1, Supporting material). Overall, the area experiences typical semi-arid Mediterranean climate conditions with annual precipitation shifting between 300 and 400 mm, with an average of 330 mm. Moderately mild temperatures, with an average over the whole year of 13.1°C, have been reported during the 1940-2007 period, reaching a maximum of 32°C in summer and a minimum of -8ºC in winter. The soils have developed on schists and quartzites and have loam and silty loam textures (average composition: 30–35% sand, 40–45% silt, 15–20% clay). The soil depth is 45–150 cm and the available soil water content is between 100 and 150 mm. The soil information was obtained from soil cartography at a scale of 1:100000 (Alias and Martinez Sanchez, 1988). The dominant soils are xerorthents regosols and the topography is characterized by steep slopes (>35%)

Field data

The forest survey was carried out in August 2014 using Field-Map instrumentation (http://www.fieldmap.cz/): 27 field plots of 11 m radius were established using a systematic, stratified sampling design. In each plot, we measured the diameter at breast height (DBH; 1.3 m above ground level) and the total height of all trees with DBH ≥ 10 cm. Two measurements, with a precision to the nearest millimeter, of DBH were made at right angles with a tree caliper (Masser BT Caliper) and the arithmetic mean was recorded. The total height was measured using a rangefinder and inclinometer (Laser Technology ForestPro Laser), with a precision to the nearest centimeter. The structure and silvicultural conditions were defined using the following stand parameters: number of trees per hectare (N), basal area per hectare (G), mean arithmetic diameter (d_m) and basal area median diameter (d_g), mean arithmetic heights (H_m), and Assmann dominant height (H_o) (Assmann, 1970) (Table S1, Supporting material).

LiDAR data and processing

The LiDAR data were acquired on April 10, 2013 by the company Heliografics Fotogrametria S.L. (Alicante, Spain), using an ALS50-II laser scanner (Leica-Geosystems AG, Heerbrugg, Switzerland) with a laser repetition rate of 158.2 kHz, a scan frequency of 100 Hz, illuminated footprint diameter of 0.32 cm, and an FOV of 12 degrees. The field was scanned by plane from a flight altitude of 3300 m.a.s.l. The ALS data were acquired with a point density of 10.5 points/m^2. They were geo-referenced in the European Terrestrial Reference System 1989 (ETRS89) coordinate system. The planimetric coordinates (x and y) and ellipsoidal height values were computed for all echoes. The time gap between the LiDAR data acquisition and the field data collection is considered insignificant according to the annual height and diameter growth in the study area (Sánchez-Salguero et al., 2012).

For this study, three diferent point densities were achieved, based on a random selection of LiDAR pulses in a grid cell of 1 m^2, and were used in the segmentation process: 10.5, 4, and 0.5 pulses m^{-2} (density). The forest-stand homegenity and geographic distribution make this statistic robust and informative. The minimun density, 0.5 pulses m^{-2}, exceeds the minimum necessary to create the 3-m DEM required under the proposed USGS specifications (USGS, National Spatial Program, 2009).

Recommendations mentioned in Ruiz et al. (2014) were followed to avoid the influence of the Digital Terrain Model (DTM) on the final results. Therefore, separate filtering processes for the three point clouds were produced, using an adapted algorithm from Kraus and Pfeifer (1998), based on linear prediction. Next, these filtered returns were used to generate DTMs with a spacing grid of 1, 2, and 5 m, respectively, for the pulse densities mentioned above (10.5, 4, and 0.5 pulses m^{-2}) (Anderson et al., 2006). In this way, equal conditions for obtaining models are guaranteed, so that point clouds of different pulse densities from different flight planning settings could be mock.

Next, the elevation values for the LiDAR data returns were normalized using the ground surface model calculated above. We computed LiDAR metrics to support regression, based on previous research by Næsset (2002). Metrics were calculated using FUSION LIDAR Toolkit (McGaughey, 2014). In this study, a total of 43 metrics were extracted from LiDAR pulses using the *gridmeetric* command. The metric were calculated from the height distribution of laser returns and they were used as regressors in the statistical analyses. To obtain a complete explanation of the FUSION tools, see McGaughey

(2014). The summary of the LiDAR metrics, with their corresponding descriptions, is shown in Table S2, Supporting material.

LiDAR data modeling

We built predictive models with the forest structural attributes and metrics obtained from the LiDAR data within each field plot. We computed multiple linear, power, and exponential regressions corresponding to all possible combinations. Linearized transformations were performed for the power and exponential regressions. Models were evaluated following the criteria: (a) statistical significance (p value<0.05), (b) minimum root-mean-squared error (RMSE), (c) minimum bias, (d) homoscedasticity, performing a Breusch-Pagan test (Herwartz, 2006), and normal distribution of residuals, verified with a Shapiro-Wilk test (Mohd Razali and Wah Yap, 2011), (e) parsimony principle, (f) non-collinearity, when more than one variable were selected, and (g) agreement with current biological knowledge (Vandekerckhove et al., 2014).

Specifically, in points (e) and (f), the variables included in the model were selected through an exhaustive search using the Bayesian information criterion (BIC) method, which performs all possible subset regressions and lists the models in ascending order of BIC. The models with the lowest BIC were selected. In addition, multicollinearity among the explanatory variables was verified with the condition index (Belsley, 1991). All the variables selected in the models had a condition index lower than 30 and a p-value of less than 5%. The accuracy of the models was assessed by performing a leave-one-out cross-validation. The resulting models were applied to the whole extent of the study area. For each model, LiDAR-based metrics were extracted from the whole point clouds, using a pixel size equivalent to the field plot size, with FUSION (McGaughey, 2014).

R software (R Core Team, 2015) and the leaps package (Thomas Lumley using Fortran code by Alan Miller, 2009) for variable selection were the tools employed.

Segmentation methods applied for stand delineation

Stands were segmented using two different algorithms that differed in their complexity. The first one was based on multiresolution segmentation using eCognition software (Trimble, 2007), involving a more complex method; the second one was based on mean shift segmentation using Orpheo ToolBox software (OTB) (CNES, 2013) for QGIS (QGIS Development Team, 2009) (Fig. 1), as a less complex approximation to compare with the eCognition results. Both algorithms used basal area per hectare (G) and Assmann dominant height (H_o) as silvicultural variables to identify and group LiDAR data into a single stand. These structural variables were chosen based on our knowledge of the forest in our study areas.

The multiresolution segmentation approach was applied as explained in Hamilton et al. (2007), using an optimization procedure which locally minimizes the average heterogeneity of image objects for a given resolution. Using multiresolution segmentation, scale parameter determines the average size of the image objects, and shape and form are determined by the input image layers which weights determine the homogeneity (Hamilton et al., 2007). Segmentations for different scale parameters were tested from a minimum value of two to an increasing number of parameters, until one unique object resulted.

The second segmentation methodology used Orpheo ToolBox software (OTB), a non-parametric density estimator based on Parzen window (Babich and Camps, 1996). It is an adaptive gradient ascent method that works by discovering local maxima in the feature-space, by moving the window towards them incrementally. With the local maxima detected, the data points can be grouped into clusters (Wu et al., 2013). Three parameters must be set: (1) the spatial radius, to define the neighborhood, (2) the range radius, to define the interval in the spectral space, and (3) the minimum size of the regions to keep after clustering.

Validation of the segmentation method and stand map analysis

The validation of an image segmentation is still a hard task (Haralick and Shapiro, 1985). An accurate segmentation is one which homogenizes regions according to a specific characteristic and, at the same time, differentiates adjacent regions according to the same characteristic (Haralick and Shapiro, 1985). Thus, segmentation should be intra-region uniform and inter-region heterogeneous. From the statistics available to validate image segmentation, Global Score - as defined in Johnson and Xie (2011) - has been selected due to its simplicity of calculation and of understanding and its good results.

Johnson and Xie (2011) suggested that the global intra-segment goodness measure should be assessed as a variance weighted by each segment area on which each variance is calculated divided by the total area: (Equation 1).

$$wVar = \frac{\sum_{i=1}^{n} a_i \cdot v_i}{\sum_{i=1}^{n} a_i} \qquad (1)$$

Where v_i is the variance and a_i is the area of the segment i. Segments with low variance should be relatively homogeneous. A weighted variance was used so that large segments had more impact on the global calculations than small ones.

As an inter-segment global goodness measure, Moran’s Index (Moran, 1950) was used. This is a measure of the spatial autocorrelation within the data and indicates the statistical separation between equal spatial objects (Kim et al., 2008) (Equation 2). The values of MI range from -1, indicating low spatial correlation and perfect dispersion, which is desirable to the resulting segmentation, to +1, representing perfect correlation. A value of zero indicates a random spatial pattern (Cliff and Ord, 1981).

$$MI = \frac{n \sum_{i=1}^{n} \sum_{j=1}^{n} w_{ij} (y_i - \bar{y})(y_j - \bar{y})}{\sum_{i=1}^{n} (y_i - \bar{y})^2 \left(\sum_{i=j} \sum w_{ij}\right)} \quad (2)$$

Where n is the total number of regions, w_{ij} is a measure of the spatial proximity, y_i is the mean spectral value of region i, and $\bar{y}$ is the mean spectral value of the image. Each weighted w_{ij} is a measure of the spatial adjacent regions.

In order to compare MI and the weighted variance, they were both normalized (Equation 3).

$$(X - X_{min}) / X_{max} - X_{min} \quad (3)$$

Where X_{min} and X_{max} are the minimum and maximum values of weighted variance or MI from all the calculations computed for every layer. Normalized values range between 0 and 1.

Finally, the Global Score is defined as the sum of the normalized weighted variance and the normalized MI (Equation 4).

$$GS = V_{norm} + MI_{norm} \quad (4)$$

Where V_{norm} is the normalized weighted variance and MI_{norm} the normalized MI. Therefore, in segmentation results, GS will range between 0 and 2, the closer to zero the better; that is, with a low weighted variance as a measure of intra-segment heterogeneity and a low MI value as a measure of inter-segment homogeneity. As there was more than one layer in the image, the GS values were averaged by the number of bands (Johnson and Xie, 2011).

Results

Assmann dominant height and basal area modeling

The stand H_o and BA models based on regression methods provided R^2 values that ranged from 0.81 to 0.97 (Table 1), with a root-mean-squared error of the cross validation (RMSECV) below 1 m for dominant height and 6 m^2 ha^{-1} for basal area. The models showed low values of bias in all cases, with consistency of the prediction models. In all cases, the exponential and power function models performed significantly better than the linear ones.

Values of R^2 greater than 0.95 and an MAE value of 0.40 m were obtained for H_o using exponential models, with an RMSECV between 0.53 m (10 pulses m^{-2}), and 0.76 m (0.5 pulses m^{-2}) (Table 1). The basal area models had trends similar to those of the dominant height models, with R^2 values higher than 0.84 and low values of RMSECV for the exponential model (3.99 m for 10 pulses m^{-2}; 5.05 m for 4 pulses m^{-2}; and 2.90 m for 0.5 pulses m^{-2}) (Table 1).

Following the independent variable data selection, the models using height variables (i.e., ElevP99, ElevCURT mean CUBE, and ElevP90 for H_o; and ElevP50, ElevMAD mode CUBE, and Elev mean for G), together with a descriptor for the density of the forest canopy (CanopyReliefRatio), were the most successful models (Fig. S2, Supporting Material).

Figure 2 presents the scatter plots of the best estimates of H_o and BA for the selected regression model versus the LiDAR values for the densities 10, 4, and 0.5 pulses m^{-2}. The predicted H_o was in near perfect agreement with the observed measurements, the R^2 value (> 0.95) being higher than that of the regression between the modeled and observed G (> 0.84).

eCognition multiresolution and OTB mean shift segmentation

The response of Multiresolution Segmentation to forest-stand delineation, described by the number of segments created, varied with the scale parameter (Tables 2 and 3). Using the eCognition segmentation algorithm, a total of 1628 segments or stands were delineated with a scale parameter of 2 (Moran´s Index MI_{norm} = 0.98 for H_o and MI_{norm} = 1.00 for G; average stand area = 0.25 ha), of which 11 were classified at the 36 scale

(MI_{norm} = 0.06 for H_o and MI_{norm} = 0.22 for G; average stand area = 37.18 ha) (Table 2). A total of 221 segments or stands were delineated using Orpheo ToolBox (OTB), with a spatial radius and a range radius of 2 and a minimum size region of 20 (MI_{norm} = 0.00 for H_o and MI_{norm} = 0.88 for G; average stand area = 1.85 ha), and 11 were classified at a spatial radius of 8, a range radius of 2, and a minimum size region of 400 (MI_{norm} = 0.05 for H_o and MI_{norm} = 0.79 for G; average stand area = 37.18 ha) (Table 3).

General trends in the behavior of the method might be detected when the Global Score is represented together with the normalized MI and the normalized variance in the range parameter (Fig. 3). Figure 3a shows the Global Score, normalized weighted variance, and normalized MI of segmentations assessed at different scale parameters for the eCognition Multiresolution segmentation (10 pulses m^{-2}). Segmentations with low normalized MI values had, at the same time, high normalized variance or *vice versa* due to the characteristics of the definition of the variables (Equations 1, 2, 3, and 4).

The Global Scores for eCognition Multiresolution segmentation were better than the results obtained with OTB Mean Shift segmentation (Fig. 4). When compared with manual delineation, eCognition Multiresolution segmentations also performed better (Fig. 4).

LiDAR pulse density effects on the segmentation process

As expected, the LiDAR pulse density affected stand delineation. We summarized these effects by analyzing the normalized weighted variance and MI values. The best point density for *P. sylvestris* stand delineation was 10 points m^{-2}, which provided the lowest values of weighted variance and the highest values of normalized MI (Fig. 5). Both methods predicted the dominant heights of the stands better than the basal area.

A one-way, between subjects ANOVA was conducted to compare the effects of pulse densities of 10, 4, and 0.5 m^{-2} on plot-measured basal area and dominant height. There were no statistically significant effects of pulse density on basal area when comparing group means at the p<0.05 level [$F_{2,\ 9595}$ = 1.15, p = 0.317]. However, there was a significant effect of pulse density on Assmann dominant height [$F_{2,\ 9595}$ = 5.69, p = 0.003]. *Post hoc* comparisons using the Tukey HSD test indicated that the mean dominant height of the segments for the pulse density of 0.5 (M = 10.56, SD = 1.21) differed significantly from that of the other groups. However, the dominant heights in the segmentation with a pulse density of 10 (M = 10.48, SD = 1.07) did not differ significantly from those of the segmentation with a pulse density of 4 (M = 10.47, SD = 1.26).

Discussion

Our results show that, given the conditions set in this study, it is possible to generate accurately *P. sylvestris* forest-stand segmentations using multiresolution or mean shift segmentation methods, even with low-pulse-density LIDAR - which is an important economic advantage for forest management. However, eCognition multiresolution methods provided better results than OTB mean shift segmentation methods for stand delineation based on dominant height and basal area estimations. Furthermore, the influence of pulse density on the results was not statistically significant in_basal area calculations. However, for low pulse density, dominant height results could be affected.

Assmann Dominant Height and Basal Area Modeling of the stand

The performance of the Assmann dominant height and basal area models compares favorably with the results of other studies in which stand height and G were modeled using LiDAR data. The coefficient of determination for the final dominant height model developed in this study (R^2 > 0.95) was in the range of previously reported values (0.82 to 0.98; Means et al., 2000; Næsset, 2002; Coops et al., 2007; Stone et al., 2011; González-Ferreiro et al., 2012; González-Ferreiro et al., 2013; Watt and Watt, 2013).

The RMSE was similar to or lower than the values reported for other coniferous species (Means et al., 2000; González-Ferreiro et al., 2013; Watt and Watt, 2013); in these studies, it was also found that exponential functions performed better than linear regression models.

Model predictions of basal area had a precision (R^2 > 0.84) comparable to that found in similar studies within coniferous forests in boreal and temperate regions. The coefficients of determination ranged from 0.62 to 0.94 for models predicting basal area in coniferous forests in the United States of America (Means et al., 2000), Norway (Næsset, 2002; Næsset et al., 2005), and Denmark (Nord-Larsen and Schumacher, 2012). Additionally, the type of explanatory variable used might cause the main differences. González-Ferreiro et al. (2013) generated models to estimate biomass, which firstly was calculated as a combination of heights and diameter. However, in our study, first order connections were assessed, as we worked directly with dominant heights, considered as the combination of the tree heights and basal area - as a diameter dependent variable, but not a combination of both variables.

Finally, the precision of dominant height and basal area models will be affected by the errors in the generation of DTM, at the height at which the point clouds are normalized, the errors of the sensor, and the pulse density (Bollandsås et al., 2013). However, variations in LiDAR pulse density did not have a significant effect on the modeling process. In fact, neither bias nor percentage error varied meaningfully (González-Ferreiro et al., 2013; Ruiz et al., 2014).

LiDAR pulse density effects on prediction models

The accuracy of the forest structure metrics slightly increased as a function of pulse density (Table 1). The determination coefficients of dominant height and basal area did not increase significantly from the lowest to the highest pulse density (i.e., from 0.5 to

10.5 pulses m^2). Further, accuracy seemed to be related more to model selection than to point density. For example, the accuracy of the exponential models for dominant height remained approximately equal to its maximum (R^2 > 0.94). Similarly, the accuracy of the power models for basal area rose steadily up to 4 pulses m^{-2} (R^2 = 0.90), then decreased to its lowest determination coefficient (R^2 = 0.81). Collectively, these results indicate that beyond a certain density level (even as low as 0.5 points m^2) accuracy does not increase significantly. These are good examples of forest metrics that require a low density to achieve reasonable accuracy, but do not benefit significantly from very high LiDAR density (Jakubowski et al., 2013). Other authors reported similar results for the modeling process, with high correlations between LiDAR metrics and forest inventory attributes at the plot level, based on low-pulse-density LiDAR (<2 pulses m^{-2}) (Thomas et al., 2006; Næsset, 2009; González-Ferreiro et al., 2013; Ruiz et al., 2014). Our results were not as accurate, most likely due to the more complex study area. This indicates that stand allometry requires a relatively lower number of LiDAR returns to be mapped accurately.

eCognition Multiresolution and Mean Shift OTB Segmentation

We found that both eCognition and OTB segmentation could be automatically segmented to produce spatial *P. sylvestris* stands and that an interpreter could label the stands in a manner similar to traditional photography (Fig. 4). These results are consistent with those achieved in other studies using LiDAR for automation of stand delineation applied to forest inventory practices (Mora et al., 2013; Dechesne et al., 2016). LiDAR data have demonstrated the utility of within-stand forest structural attributes (e.g., current dominant stand height and basal area) as a subset of attributes required for characterization of forest stands.

The high Global Score, normalized weighted variance, and normalized MI of the segmentations indicate that both eCognition Multiresolution and OTB segmentations detected homogenous stands well, in concordance with previous work (Espindola et al., 2006; Johnson and Xie, 2011). Further, the eCognition Multiresolution segmentation at 10 pulses m^{-2} was the best scored segmentation, giving intra-region uniformity but inter-region heterogeneity. The reason for that could be that the eCognition Multiresolution segmentation algorithm was formulated to search for both intra-region homogeneity and inter-region heterogeneity, while the Mean-Shift algorithm was designed to search only for homogenous regions (Baatz and Schäpe, 2000). As deduced from Figure 3, the value of the scale parameter had a direct effect on the number of polygons produced by the resulting segmentation. In contrast, OTB Mean-Shift segmentation stands were usually detected and delineated correctly, but the number of segments was lower and did not always match those of the ground reference data.

Due to the relatively large size and homogeneity of the study area used, in comparison with other studies (Espindola et al., 2006; Johnson and Xie, 2011), we found values of the Global Score that represented less than 5% of the difference in score between the first minimum and the next minimum value, suggesting that there is no single best segmentation but multiple ones; which can differ in the number and size of the segments. Because the number of segments depends on the study area surface and the size of the forest stands (O'Hara and Nagel, 2013), the best results could be identified as the best minimum group of values of Global Scores, normalized weighted variance, normalized MI, and number of segments (Chen et al., 2014). These values are located around the crossing point of the curves of normalized weighted variance and normalized MI (Figures 3 and 5).

Furthermore, there should be agreement between the segmentation with the best Global Score, better normalized weighted variances, and better normalized MI and the resulting number of segments, depending on the forest management objectives. For precision silviculture, foresters may require very precise stand delineation regarding intra-region variance with a high number of segments, despite the similarity of the segments to each other; for example, segmentation at scale parameter 6 in Table 2, even when it is not the one with the best score. However, in Mediterranean pine forests, where protection and water management are the main silvicultural targets, a less precise stand delineation would be demanded, including larger areas of high inter-region heterogeneity - with, consequently, a low number of segments (e.g., segmentation at scale parameter 10 in Table 2), although with higher intra-region variance (Kim et al., 2008; Johnson and Xie, 2011).

The Mean Shift segmentation algorithm showed the additional complexity of using three parameters (the range, spatial radius, and minimum region size) in the segmentation process. In the analysis of the Mean Shift segmentations, more unreliability of the validation system was detected. No obvious relationship between the segment number created and the Global Score values could be observed (Fig. 5). Consequently, selection of the best segmentation for forest-stand delineation using OTB methodology is not as straightforward as previously thought. Given that the Mean Shift algorithm has been proven as an adequate method for forest-stand delineation (Wu et al., 2013, 2014), the disturbances in the detection of the best segmentation may come from the validation system - which, we suggest, should be rethought for this kind of technique with multi-dependent variables.

The question that then arises is: what benefit derives from the cost and effort of the eCognition Multiresolution Segmentation approach presented herein, when the results are similar to those obtained using OTB? Moreover, OTB implementation for stand delineation would likely be simpler, more cost-effective, and of similar accuracy. While dominant stand height and basal area do not constitute the entirety of an inventory, each is amongst the more important of the suite of attributes that is generated. Dominant stand height information is important for management purposes and is indicative of site conditions, while basal area (related to volume or biomass) is key to forest management (silvicultural treatments) and carbon-related considerations. A recommendation for the future is that eCognition methodology (and related semi-automated processing approachs) should remain focused on locations where precision silviculture inventory programs persist. On the other hand, segmentation provided by OTB methodology, offering less precision but also compatibility and similarity of stand delineation, should be used in extensive silviculture (e.g., protection, climatic change adaptation, and hydrologically-oriented silviculture). For areas that are not subject to regular management or monitoring activities, it is possible that the more limited precision of stand delineation provided by OTB will prove sufficient for many monitoring and reporting needs. Thus, a stratification of activity may be possible based upon the monitoring requirements associated with a given area.

LiDAR pulse density effects on the segmentation process

The segmentation algorithms were also influenced by the LiDAR pulse density. Our results suggest that basal area is not affected by segmentations based on different LiDAR pulse densities. In contrast, low pulse density affects the estimation of dominant height. Segmentations using medium and high pulse densities do not appear to be significantly affected with respect to dominant height results. However, it should be noted that the values of the means and standard deviations for dominant height were similar among the three pulse density approaches.

Overall, our results indicate that a very high LiDAR pulse density may not be necessary to predict typical forest structure metrics at the plot scale or for stand delineation. These findings are particularly important for land managers that need to survey a large area with a specific forest metric and accuracy in mind. Our results, considered in terms of cost, coverage, and density, can help guide this process. For example, if dominant basal area is the most important metric to estimate at a reasonable accuracy level, it may be sufficient to acquire LiDAR data at about 1 pulse m^{-2}. On the other hand, if it is critical to derive the average dominant height with high accuracy, then it may be advisable to use a much higher pulse density - between 2 and 4 pulses m^{-2}.

Conclusions

The objective of this study was to use LiDAR data segmentation to produce stand-level predictions of dominant height and basal area as well as to use two different segmentation techniques for stand delineation oriented to *Pinus sylvestris* forest management in Mediterranean mountains. The use of LiDAR data provided a large sample appropriate for model calibration and independent validation of attribute predictions. We have demonstrated the utility of LiDAR data with regard to estimating dominant stand height and basal area with an accuracy suitable for operational activities. We have also noted the differences in stand delineation (number and form) between two different segmentation algorithms (eCognition and OBT), using a semi-automated methodology based on forestry attributes in a Mediterranean environment. We did not find significant differences between high and low LiDAR pulse density, neither in the creation of prediction models for dominant height and basal area nor in the segmentation process. Nevertheless, for further assertions, more comparative studies - varying the radius of the plot sample - should be carried out. The technique developed in this project could be implemented to provide more precise data for forest management. We propose that the approach shown here should be considered for stand delineation in other large *Pinus* plantations in Mediterranean regions with similar characteristics. Further, large-area, wall-to-wall characterization with a high level of attribute detail is difficult to obtain, with sampling offering a practical, robust, and reliable alternative. Future global forest inventory programs may benefit from consideration of the framework and methods presented herein. Also, depending on the location and attributes required, wall-to-wall mapping that integrates high-spatial-resolution sensors (i.e., RapidEye or World-View) with LiDAR data may provide a powerful opportunity for systematic and repeatable monitoring and reporting of silvicultural activities.

Acknowledgements

We are grateful for support from the project ThermoLiDAR "A new tool for sustainable forest management based on LiDAR (Laser Imaging Detection And Ranging) and THERMAL data integration" FP7-SME-2012-315165) (Seventh Framework Programme of the European Union) and the project LIFE13 ENV/ES/001384 "Development of technical guidelines for carbon sequestration and dynamization of carbon compensation in forests". We also acknowledge financial and institutional support from the University of Córdoba-Campus de Excelencia CEIA$_3$. We thank Miguel Lara for his support during field data collection and his insights into the development of the forest structural attributes from the LiDAR metrics.

References

Alias, L.J., Martinez Sanchez, J., 1988. Xerochrepts from the Orce and Maria Sierras (Granada y Almeria). Anales de Edafologia y Agrobiologia (Spain).

Anderson, E.S., Thompson, J.A., Crouse, D.A., Austin, R.E., 2006. Horizontal resolution and data density effects on remotely sensed LIDAR-based DEM. Geoderma 132, 406-415.

Assmann, E., 1970. Principles of forest yield study.

Baatz, M., Schäpe, A., 2000. Multiresolution segmentation: an optimization approach for high quality multi-scale image segmentation. Angewandte Geographische Informationsverarbeitung XII 58, 12-23.

Babich, G.A., Camps, O.I., 1996. Weighted Parzen windows for pattern classification. IEEE Transactions on Pattern Analysis and Machine Intelligence 18, 567-570.

Belsley, D., 1991. A Guide to using the collinearity diagnostics. Computer Science in Economics and Management 4, 33-50.

Blaschke, T., Hay, G.J., Kelly, M., Lang, S., Hofmann, P., Addink, E., Queiroz Feitosa, R., van der Meer, F., van der Werff, H., van Coillie, F., Tiede, D., 2014. Geographic Object-Based Image Analysis – Towards a new paradigm. ISPRS Journal of Photogrammetry and Remote Sensing 87, 180-191.

Bollandsås, O.M., Maltamo, M., Gobakken, T., Næsset, E., 2013. Comparing parametric and non-parametric modelling of diameter distributions on independent data using airborne laser scanning in a boreal conifer forest. Forestry 86, 493-501.

Bouvier, M., Durrieu, S., Fournier, R.A., Renaud, J.-P., 2015. Generalizing predictive models of forest inventory attributes using an area-based approach with airborne LiDAR data. Remote Sensing of Environment 156, 322-334.

Burnett, C., Blaschke, T., 2003. A multi-scale segmentation/object relationship modelling methodology for landscape analysis. Ecological modelling 168, 233-249.

Centeno, J.A.S., Antunes, A.F.B., Trevizan, S., Correa, F., 2003. Mapeamento de áreas permeáveis usando uma metodologia orientada a regiões e imagens de alta resolução. Revista Brasileira de Cartografia 1.

Cliff, A.D., Ord, J.K., 1981. Spatial processes: models & applications. Pion London.

CNES, 2013. Orfeo Toolbox in: Program, O.A. (Ed.), 3.18.1 ed.

Coops, N.C., Hilker, T., Wulder, M.A., St-Onge, B., Newnham, G., Siggins, A., Trofymow, J.T., 2007. Estimating canopy structure of Douglas-fir forest stands from discrete-return LiDAR. Trees 21, 295-310.

Costa, G., Feitosa, R.Q., Fonseca, L.M.G., Oliveira, D.A.B., Ferreira, R.S., Castejon, E.F., 2010. Knowledge-based interpretation of remote sensing data with the InterIMAGE system: major characteristics and recent developments, Proceedings of the 3rd GEOBIA.

Chen, J.-Y., Lin, C.-H., Hsu, P.-C., Chen, C.-H., 2014. Point Cloud Encoding for 3D Building Model Retrieval. IEEE Transactions on Multimedia 16, 337-345.

Chi, H.-M., Ersoy, O.K., 2005. A statistical self-organizing learning system for remote sensing classification. Geoscience and Remote Sensing, IEEE Transactions on 43, 1890-1900.

Dechesne, C., Mallet, C., Le Bris, A., Gouet, V., Hervieu, A., 2016. Forest Stand Segmentation Using Airborne LIDAR Data and Very High Resolution Multispectral Imagery. ISPRS-International Archives of the Photogrammetry, Remote Sensing and Spatial Information Sciences, 207-214.

Espindola, G., Câmara, G., Reis, I., Bins, L., Monteiro, A., 2006. Parameter selection for region-growing image segmentation algorithms using spatial autocorrelation. International Journal of Remote Sensing 27, 3035-3040.

González-Ferreiro, E., Diéguez-Aranda, U., Miranda, D., 2012. Estimation of stand variables in Pinus radiata D. Don plantations using different LiDAR pulse densities. Forestry 85, 281-292.

González-Ferreiro, E. M., Miranda, D., Barreiro-Fernandez, L., Bujan, S., Garcia-Gutierrez, J., & Dieguez-Aranda, U. (2013). Modelling stand biomass fractions in Galician Eucalyptus globulus plantations by use of different LiDAR pulse densities. Forest Systems, 22(3), 510-525.

Hamilton, R., Megown, K., Mellin, T., Fox, I., 2007. Guide to automated stand delineation using image segmentation. RSAC-0094-RPT1. Salt Lake City, UT: USDA Forest Service, Remote Sensing Applications Center.

Haralick, R.M., Shapiro, L.G., 1985. Image Segmentation Techniques, pp. 2-9.

Herwartz, H., 2006. Testing for random effects in panel data under cross sectional error correlation—A bootstrap approach to the Breusch Pagan test. Computational statistics & data analysis 50, 3567-3591.

Jakubowski, M.K., Guo, Q., Kelly, M., 2013. Tradeoffs between lidar pulse density and forest measurement accuracy. Remote Sensing of Environment 130, 245-253.

James, G., Witten, D., Hastie, T., 2014. An Introduction to Statistical Learning: With Applications in R. Taylor & Francis.

Johnson, B., Xie, Z., 2011. Unsupervised image segmentation evaluation and refinement using a multi-scale approach. ISPRS Journal of Photogrammetry and Remote Sensing 66, 473-483.

Kim, M., Madden, M., Warner, T., 2008. Estimation of optimal image object size for the segmentation of forest stands with multispectral IKONOS imagery, Object-based image analysis. Springer, pp. 291-307.

Kraus, K., Pfeifer, N., 1998. Determination of terrain models in wooded areas with airborne laser scanner data. ISPRS Journal of Photogrammetry and Remote Sensing 53, 193-203.

Leckie, D.G., Gougeon, F.A., Walsworth, N., Paradine, D., 2003. Stand delineation and composition estimation using semi-automated individual tree crown analysis. Remote Sensing of Environment 85, 355-369.

Lopatin, J., Galleguillos, M., Fassnacht, F.E., Ceballos, A., Herna, x, ndez, J., 2015. Using a Multistructural Object-Based LiDAR Approach to Estimate Vascular Plant Richness in Mediterranean Forests With Complex Structure. Geoscience and Remote Sensing Letters, IEEE 12, 1008-1012.

Magnussen, S., Næsset, E., Gobakken, T., Frazer, G., 2012. A fine-scale model for area-based predictions of tree-size-related attributes derived from LiDAR canopy heights. Scandinavian Journal of Forest Research 27, 312-322.

Magnusson, M., Fransson, J.E., Holmgren, J., 2007. Effects on estimation accuracy of forest variables using different pulse density of laser data. Forest Science 53, 619-626.

Martín-Alcón, S., Coll, L., De Cáceres, M., Guitart, L., Cabré, M., Just, A., González-Olabarría, J.R., 2015. Combining aerial LiDAR and multispectral imagery to assess postfire regeneration types in a Mediterranean forest. Canadian Journal of Forest Research 45, 856-866.

McGaughey, R., 2014. FUSION/LDV: software for LIDAR data analysis and visualization. USDA Forest Service. Pacific Northwest Research Station.

McRoberts, R.E., Liknes, G.C., Domke, G.M., 2014. Using a remote sensing-based, percent tree cover map to enhance forest inventory estimation. Forest Ecology and Management 331, 12-18.

Means, J.E., Acker, S.A., Fitt, B.J., Renslow, M., Emerson, L., Hendrix, C.J., 2000. Predicting forest stand characteristics with airborne scanning lidar. Photogrammetric Engineering and Remote Sensing 66, 1367-1372.

Mohd Razali, N., Wah Yap, B., 2011. Power comparisons of Shapiro-Wilk, Kolmogorov-Smirnov, Lilliefors, and Anderson-Darling test. Journal of Statistical Modeling and Analytics 2, 21-33.

Mora, B., Wulder, M.A., White, J.C., Hobart, G., 2013. Modeling stand height, volume, and biomass from very high spatial resolution satellite imagery and samples of airborne LiDAR. Remote Sensing 5, 2308-2326.

Moran, P.A., 1950. Notes on continuous stochastic phenomena. Biometrika, 17-23.

Næsset, E., 2002. Predicting forest stand characteristics with airborne scanning laser using a practical two-stage procedure and field data. Remote Sensing of Environment 80, 88-99.

Næsset, E., 2009. Effects of different sensors, flying altitudes, and pulse repetition frequencies on forest canopy metrics and biophysical stand properties derived from small-footprint airborne laser data. Remote Sensing of Environment 113, 148-159.

Næsset, E., Bollandsås, O.M., Gobakken, T., 2005. Comparing regression methods in estimation of biophysical properties of forest stands from two different inventories using laser scanner data. Remote Sensing of Environment 94, 541-553.

Nord-Larsen, T., Schumacher, J., 2012. Estimation of forest resources from a country wide laser scanning survey and national forest inventory data. Remote Sensing of Environment 119, 148-157.

O'Hara, K.L., Nagel, L.M., 2013. The Stand: Revisiting a Central Concept in Forestry. Journal of Forestry 111, 335-340.

Pekkarinen, A., 2004. Image segmentation in multi-source forest inventory. Finnish Forest Research Institute, Vantaa Research Centre.

QGIS Development Team, 2009. QGIS Geographic Information System. Open Source Geospatial Foundation.

R Core Team, 2015. R: A Language and Environment for Statistical Computing, 3.2.1 ed. R Foundation for Statistical Computing, Vienna, Austria.

Radoux, J., Defourny, P., 2007. A quantitative assessment of boundaries in automated forest stand delineation using very high resolution imagery. ForestSAT Special Issue ForestSAT 2005 Conference "Operational tools in forestry using remote sensing techniques" 110, 468-475.

Ruiz, L., Hermosilla, T., Mauro, F., Godino, M., 2014. Analysis of the Influence of Plot Size and LiDAR Density on Forest Structure Attribute Estimates. Forests 5, 936-951.

Sagerer, G., Niemann, H., 2013. Semantic networks for understanding scenes. Springer Science & Business Media.

Sánchez-Salguero, R., Navarro-Cerrillo, R.M., Swetnam, T.W., Zavala, M.A., 2012. Is drought the main decline factor at the rear edge of Europe? The case of southern Iberian pine plantations. Forest Ecology and Management 271, 158-169.

Stone, C., Penman, T.D., Turner, R., 2011. Determining an optimal model for processing lidar data at the plot level: results for a Pinus radiata plantation in New South Wales, Australia.

Thomas Lumley using Fortran code by Alan Miller, 2009. leaps: regression subset selection.

Thomas, V., Treitz, P., McCaughey, J.H., Morrison, I., 2006. Mapping stand-level forest biophysical variables for a mixedwood boreal forest using lidar: an examination of scanning density. Canadian Journal of Forest Research 36, 34-47.

Trimble, 2007. Definiens Developer, 7 ed.

Vandekerckhove, J., Matzke, D., Wagenmakers, E.-J., 2014. Model comparison and the principle of parsimony. Oxford Handbook of Computational and Mathematical Psychology. Oxford University Press, Oxford.

Watt, P., Watt, M.S., 2013. Development of a national model of Pinus radiata stand volume from LiDAR metrics for New Zealand. International Journal of Remote Sensing 34, 5892-5904.

Webb, A.R., 2003. Statistical pattern recognition. John Wiley & Sons.

Wu, Z., Heikkinen, V., Hauta-Kasari, M., Parkkinen, J., Tokola, T., 2013. Forest Stand Delineation Using a Hybrid Segmentation Approach Based on Airborne Laser Scanning Data, in: Kämäräinen, J.-K., Koskela, M. (Eds.), Image Analysis. Springer Berlin Heidelberg, pp. 95-106.

Wu, Z., Heikkinen, V., Hauta-Kasari, M., Parkkinen, J., Tokola, T., 2014. ALS data based forest stand delineation with a coarse-to-fine segmentation approach, Image and Signal Processing (CISP), 2014 7th International Congress on. IEEE, pp. 547-552.

Yogamangalam, B.K.R., Karthikeyan, B., 2013. Segmentation Technique Comparison in Image Processing. IJET (ISSN: 0975-4024) 5, 307-313.

Zhong, P., Zhang, P., Wang, R., 2008. Dynamic learning of SMLR for feature selection and classification of hyperspectral data. Geoscience and Remote Sensing Letters, IEEE 5, 280-284.

Figure **1**: Flowchart of the modeling and image processing for proposed stand delimitation methodology based dominant height and basal area using LiDAR data.

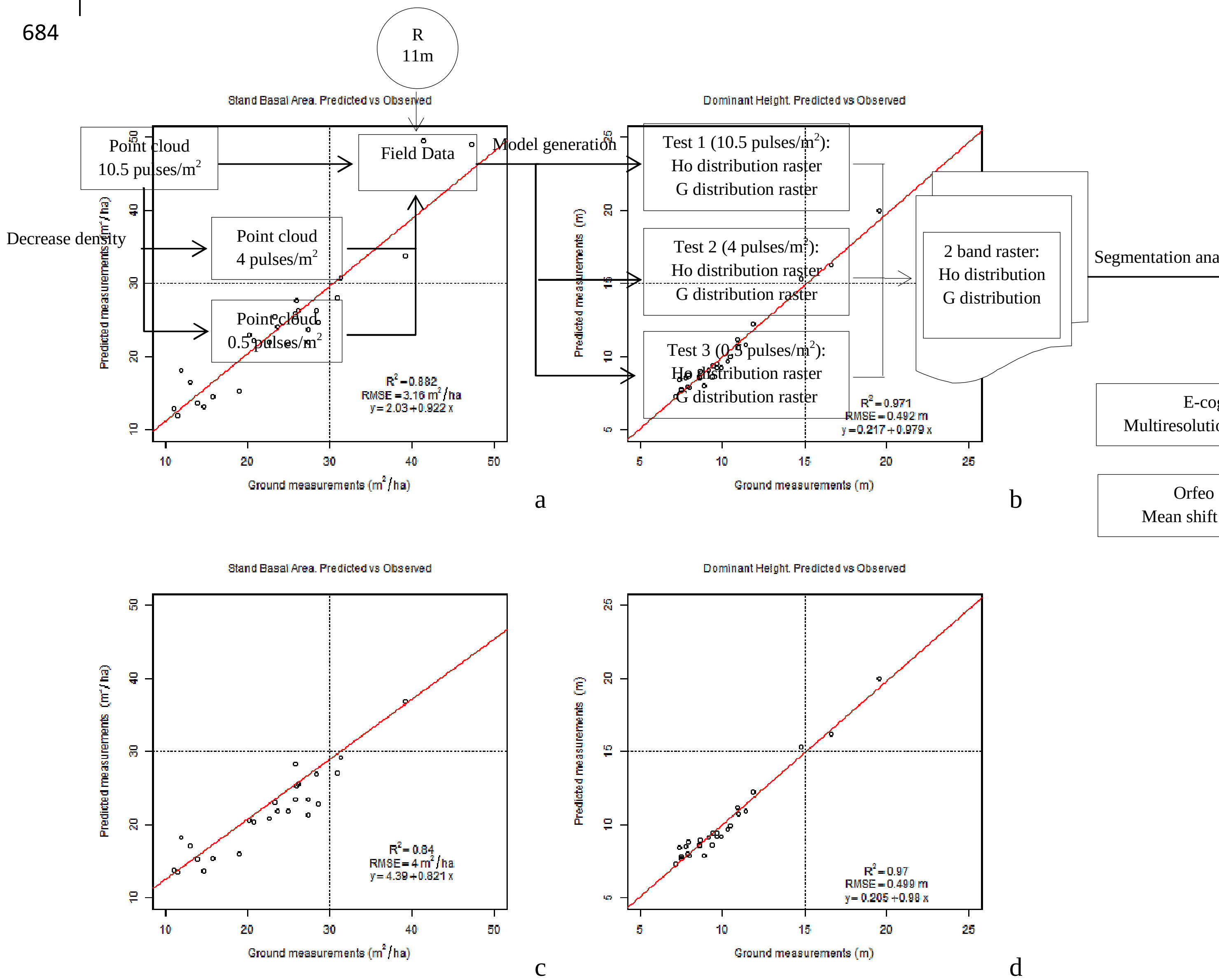

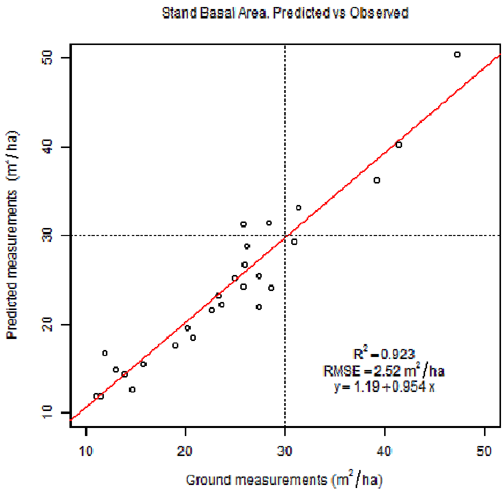

e

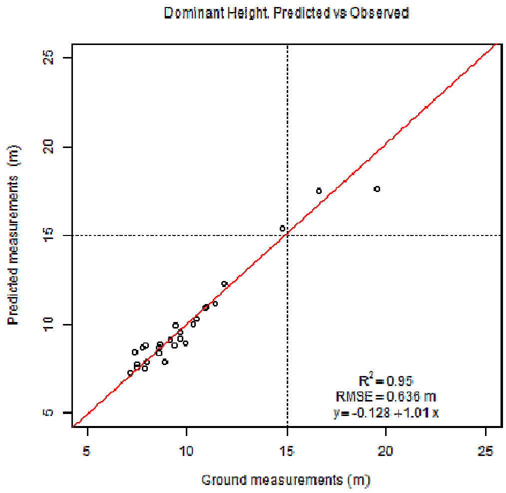

f

Figure 2: Scatter plot of the best estimated stand basal area (AB) (a, b, e) and dominate heights (H_o) (b, c, f) versus LiDAR values according to density pulses (10, 4 and 0.5 pulses/$m^2$from upper to lower figure). 1/1 Red line.

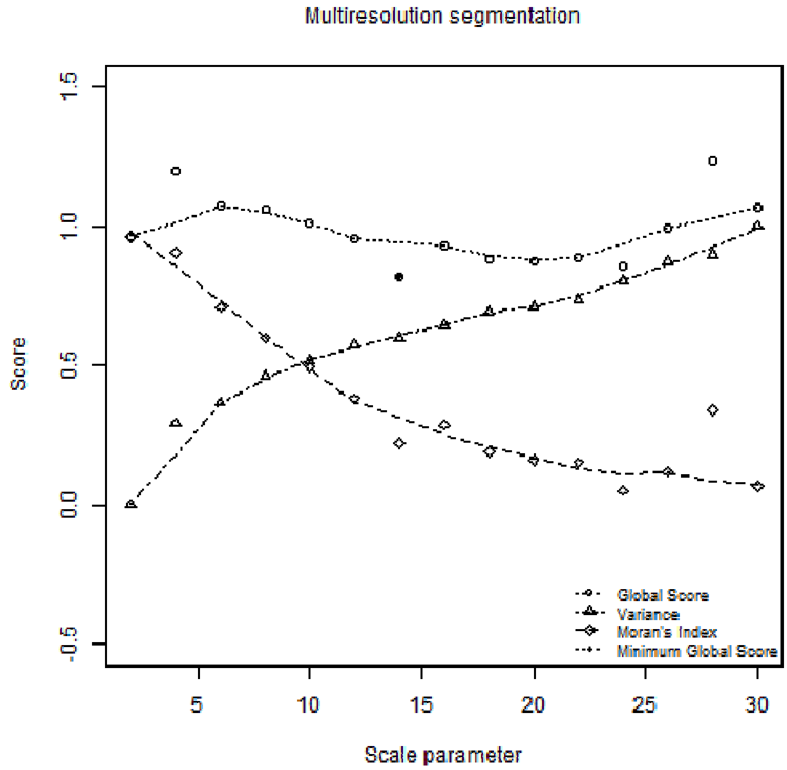

a

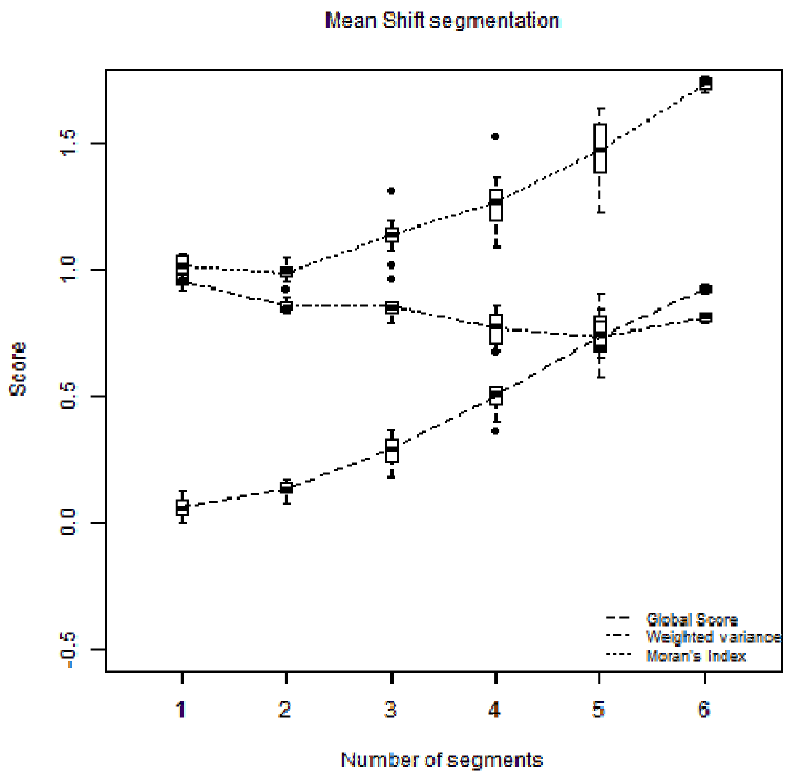

b

Figure 3: Global Score, normalized weighted variance and normalized Moran's Index for the evaluation of the segmentations a) for the eCognition's Multiresolution

segmentation at 10 pulse density; b) for the OTB Mean Shift segmentation at 10 pulse density.

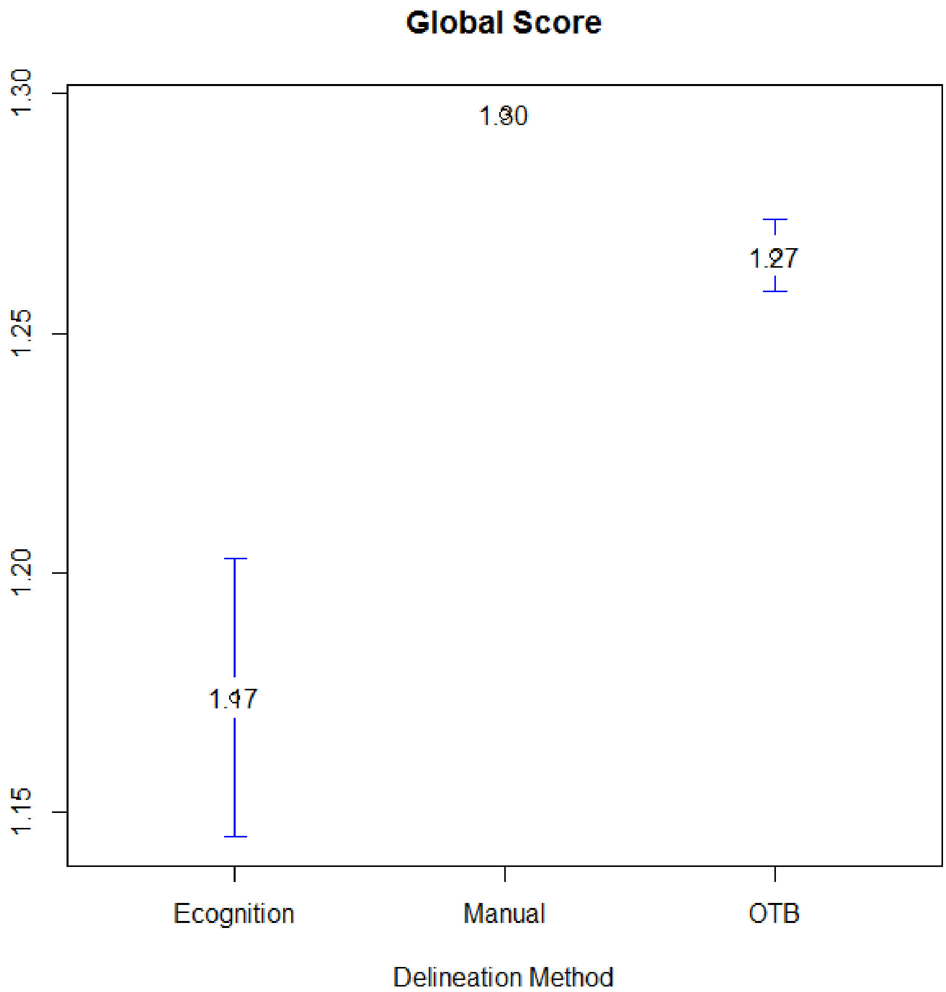

Figure 4: Mean Global Score values obtained using semi-automatic forest stand delineation at 10 pulse·m^{-2} density for Ecognition's Multiresolution segmentation, OTB Mean-Shift segmentation and manual delineation

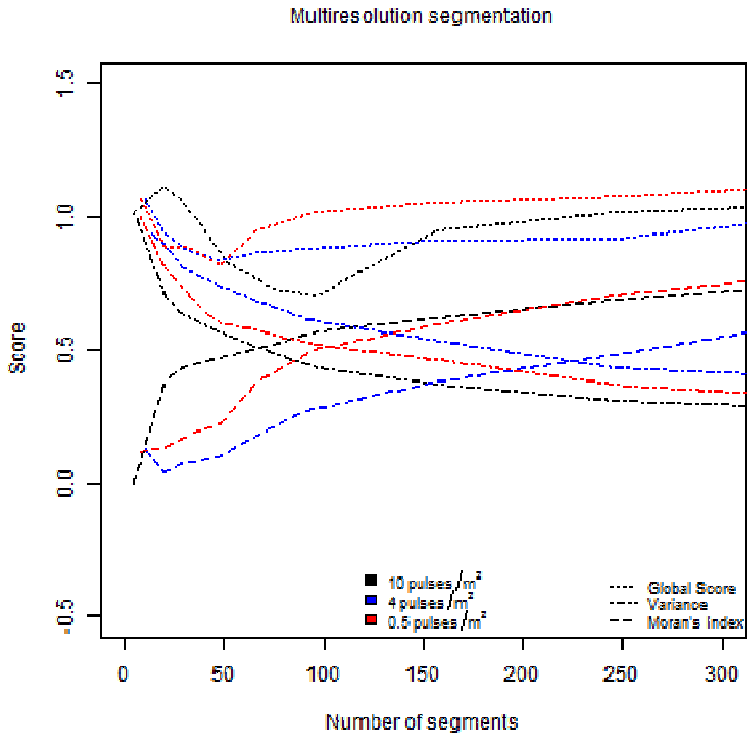

a

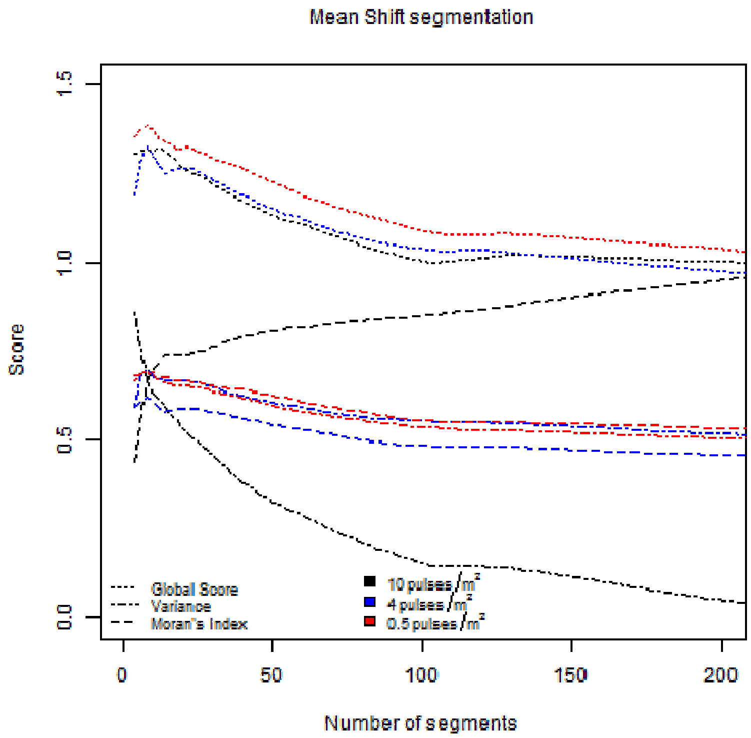

b

Figure 5: a) Normalized weighted variance, normalized Moran's Index and global scores for segmentations at 10, 4 and 0.5 pulse·m^{-2} density with eCognition's Multiresolution Segmentation, b) Normalized weighted variance, normalized Moran's Index and global scores for segmentations at 10, 4 and 0.5 pulse·m^{-2} density with Mean Shift Segmentation with OTB.

Figure 6. Maps obtained using semi-automatic forest stand delineation at 10 pulse·m^{-2} density a) Multiresolution segmentation; b) Mean-Shift segmentation

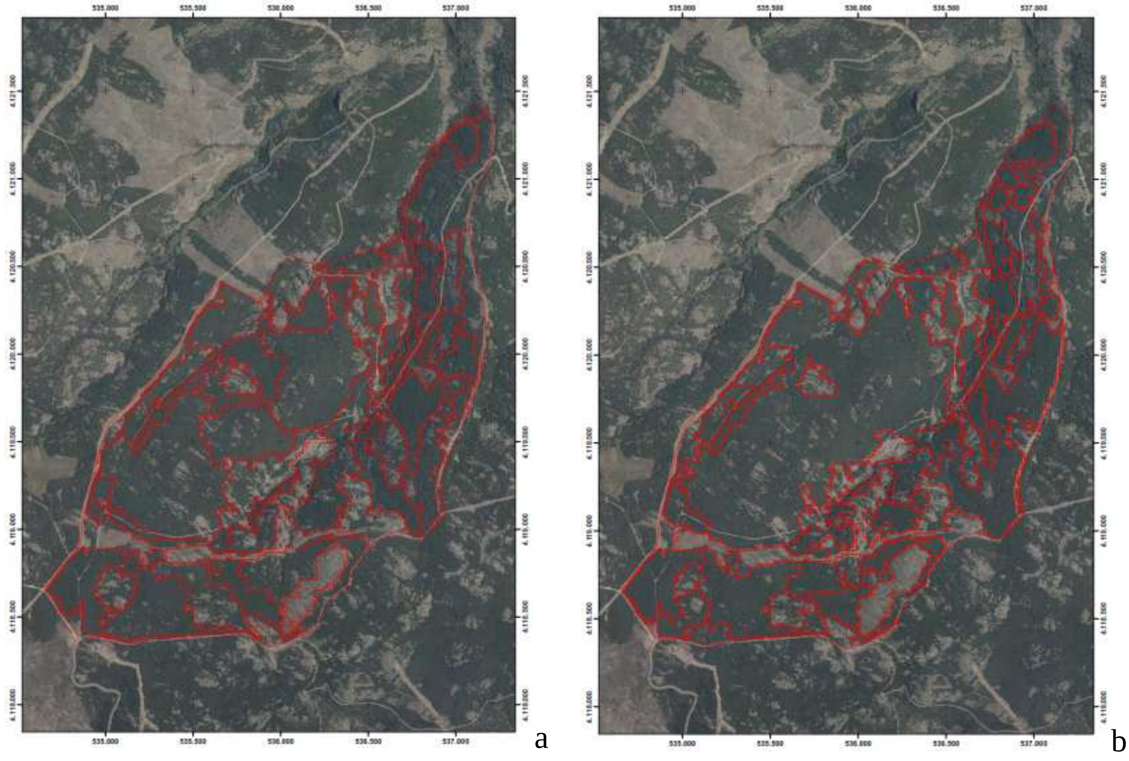

Table 1: Summary of the statistical criteria computed for evaluation the models for dominant height (H_o) and basal area (BA).

LiDAR pulse density (m^{-2})	Type of regression	Variable	R^2	BIAS	MAE	RMSE	RMSECV	%ERROR
				Dominant height (m)				
10	Lineal	Ho	0.97	$-3.7e^{-5}$	0.35	0.59	0.63	5.65
10	Exponential	Ho	**0.97**	**-0.01**	**0.40**	**0.49**	**0.53**	**5.35**
10	Power	Ho	0.94	0.03	0.50	0.62	0.79	7.89
4	Lineal	Ho	0.96	$-1.6e^{-4}$	0.44	0.56	0.64	6.44
4	Exponential	Ho	**0.97**	$\mathbf{-9.6e^{-3}}$	**0.40**	**0.50**	**0.54**	**5.54**
4	Power	Ho	0.95	$-2.9e^{-2}$	0.47	0.62	0.73	6.23
0.5	Lineal	Ho	0.93	$3.6e^{-6}$	0.59	0.78	0.94	7.78
0.5	Exponential	Ho	**0.95**	$\mathbf{2.0e^{-2}}$	**0.40**	**0.64**	**0.76**	**6.37**
0.5	Power	Ho	0.94	$-2.6e^{-2}$	0.56	0.70	0.90	7.04
				Basal area (m^2 ha^{-1})				
10	Lineal	G	0.92	$2.3e^{-5}$	3.60	3.48	3.82	10.28
10	Exponential	G	**0.88**	**-0.15**	**2.43**	**3.16**	**3.99**	**9.85**
10	Power	G	0.81	-0.14	3.11	3.90	4.58	16.15
4	Lineal	**G**	0.92	$-4.3e^{-4}$	3.09	4.46	5.75	11.38
4	Exponential	G	**0.84**	$\mathbf{-9.0e^{-2}}$	**2.95**	**4.00**	**5.05**	**10.60**
4	Power	G	0.93	-0.13	2.98	4.46	5.67	16.19
0.5	Lineal	G	0.93	$-1.8e^{-4}$	2.70	2.81	2.96	10.20
0.5	Exponential	G	**0.92**	$\mathbf{-9.1e^{-2}}$	**2.01**	**2.52**	**2.90**	**10.46**
0.5	Power	G	0.87	-0.14	2.63	3.12	3.39	12.95

Mean Absolute Error (MAE), Mean Squared Error of Cross Validation (MSECV), Root Mean Squared Error of Cross Validation (RMSECV) and percentage of error (%ERROR)

Table 2: Normalized variance (V_{norm}), normalized Moran's Index (MI_{norm}) and global scores (GS) for all scale-parameter segmentations with theirs resulting number of segments for the 10 pulse density approach. eCognition's Multiresolution segmentation approach.. Ordering indexes for two-band average values are shown in brackets. Minimum values Global Score are highlighted.

Scale Parameter	Ho 10-pulse/m^2 density band			G 10-pulse/m_2 density band			Two-band average			Number of segments
	V_{norm}	MI_{norm}	GS	V_{norm}	MI_{norm}	GS	V_{norm}	MI_{norm}	GS	
2	0,00	0,98	0,98	0,00	1,00	1,00	0,00	0,99	0,99(11)	1628
4	0,35	1,00	1,35	0,29	0,68	0,98	0,32	0,84	1,17(18)	541
6	0,44	0,54	0,99	0,42	0,40	0,83	0,43	0,47	**0,91(6)**	246
8	0,50	0,47	0,97	0,52	0,35	0,88	0,51	0,41	**0,92(7)**	154
10	0,61	0,24	0,85	0,61	0,27	0,89	0,61	0,26	**0,87(3)**	92
12	0,65	0,23	0,89	0,69	0,20	0,90	0,67	0,22	**0,90(5)**	68
14	0,71	0,07	0,79	0,76	0,07	0,83	0,73	0,07	**0,81(1)**	47
16	0,78	0,13	0,91	0,83	0,00	0,83	0,80	0,06	**0,87(2)**	30
18	0,78	0,11	0,90	0,83	0,04	0,88	0,81	0,07	**0,89(4)**	29
20	0,85	0,03	0,88	0,92	0,05	0,97	0,88	0,04	**0,93(9)**	20
22	0,85	0,03	0,88	0,92	0,05	0,97	0,88	0,04	0,93(10)	20
24	0,87	0,02	0,89	0,93	0,03	0,96	0,90	0,02	**0,93(8)**	19
26	0,89	0,03	0,93	0,98	0,08	1,06	0,94	0,05	0,99(12)	16
28	0,90	0,02	0,92	0,98	0,11	1,10	0,94	0,07	1,01(14)	15
30	0,90	0,00	0,90	0,98	0,12	1,11	0,94	0,06	1,00(13)	14
32	0,92	0,03	0,95	0,99	0,24	1,23	0,95	0,13	1,09(15)	12
34	0,92	0,03	0,95	0,99	0,24	1,23	0,95	0,13	1,09(16)	12
36	1,00	0,06	1,06	1,00	0,22	1,22	1,00	0,14	1,14(17)	11

Table 3: Normalized variance (V_{norm}), normalized Moran's Index (MI_{norm}) and global scores (GS) for all spatial radius, rage radius and minimum size of the region segmentations with theirs resulting number of segments for the 10 pulse density approach. OTB Mean Shift segmentation approach. This is an extract of the 20 best global-scored segmentations out of 278. Ordering indexes for two-band average values are shown in brackets. Minimum values of Global Score are highlighted.

Spatial radius	**Rage Radius**	**Min size of region**	**Ho 10-pulse/m^2 density band**			**G 10-pulse/m$_2$ density band**			**Two-band average**			**Number segments**
			V_{norm}	**MI_{norm}**	**GS**	**V_{norm}**	**MI_{norm}**	**GS**	**V_{norm}**	**MI_{norm}**	**GS**	
2	2	20	0,00	0,00	0,00	0,97	0,88	1,85	0,48	0,44	**0,92(4)**	221
2	2	1000	0,55	0,31	0,87	0,27	0,48	0,76	0,41	0,40	**0,819(2)**	6
2	12	20	0,71	0,91	1,63	0,00	0,00	0,00	0,35	0,45	**0,81(1)**	5
4	2	20	0,03	0,03	0,06	0,95	0,88	1,84	0,49	0,45	**0,95(7)**	199
4	2	50	0,23	0,19	0,42	0,81	0,74	1,56	0,52	0,46	0,99(11)	97
6	2	20	0,06	0,00	0,06	0,95	0,88	1,83	0,50	0,44	**0,95(6)**	198
6	2	50	0,28	0,17	0,46	0,83	0,75	1,58	0,55	0,46	1,02(19)	86
8	2	20	0,10	0,07	0,18	1,00	0,85	1,85	0,55	0,46	1,01(18)	195
8	2	400	0,53	0,30	0,83	0,56	0,61	1,18	0,54	0,46	1,00(15)	11
8	4	20	0,14	0,05	0,19	0,89	0,79	1,69	0,52	0,42	**0,94(5)**	116
8	4	50	0,29	0,12	0,41	0,80	0,70	1,51	0,55	0,41	**0,96(8)**	62
10	2	20	0,09	0,03	0,12	0,96	0,91	1,88	0,53	0,47	1,00(14)	187
10	4	20	0,07	0,11	0,18	0,93	0,80	1,74	0,50	0,45	**0,96(9)**	118
10	4	1000	0,58	0,43	1,02	0,41	0,55	0,97	0,50	0,49	0,99(13)	5
12	2	20	0,08	0,08	0,16	0,99	0,88	1,88	0,53	0,48	1,02(20)	192
12	4	20	0,17	0,12	0,29	0,93	0,76	1,69	0,55	0,44	0,99(12)	108
14	2	20	0,01	0,04	0,06	0,92	0,84	1,76	0,47	0,44	**0,91(3)**	180
16	2	20	0,12	0,09	0,22	0,95	0,85	1,80	0,53	0,47	1,01(16)	181
16	4	20	0,16	0,15	0,32	0,89	0,72	1,61	0,53	0,43	0,96(10)	94
18	2	20	0,12	0,07	0,20	0,95	0,87	1,82	0,54	0,47	1,01(17)	179